Experimental and Computational Insights into the Anomalous Thermal Expansion of $(NH_4)ReO_4$

Matilde Saura-Múzquiz[1,2], Bryce G. Mullens[1], Max Avdeev[1,3], Prathap K. Jharapla[4], G. Vaitheeswaran[5*], M. K. Gupta[6,7], R. Mittal[6,7], Brendan J. Kennedy[1*]

[1] School of Chemistry, The University of Sydney, Sydney, New South Wales 2006, Australia

[2] Department of Materials Physics, Universidad Complutense de Madrid, 28040, Madrid, Spain

[3] Australian Nuclear Science and Technology Organisation, New Illawarra Road, Lucas Heights, New South Wales 2234, Australia

[4] Advanced Centre of Research in High Energy Materials (ACRHEM), University of Hyderabad, Prof. C. R. Rao Road, Gachibowli, Hyderabad, 500046, Telangana, India

[5] School of Physics, University of Hyderabad, Prof. C. R. Rao Road, Gachibowli, Hyderabad, 500046, Telangana, India

[6] Solid State Physics Division, Bhabha Atomic Research Center, Mumbai, 400085, India

[7] Homi Bhabha National Institute, Anushaktinagar, Mumbai, 400094, India

[*] Corresponding Authors: G. Vaitheeswaran (vaithee@uohyd.ac.in) Brendan J. Kennedy (brendan.kennedy@sydney.edu.au)

Keywords: Scheelite; Neutron Diffraction; Thermal Expansion; Density Functional Theory; Raman Spectroscopy

Abstract

The temperature dependence of the structure and the ground state properties of scheelite type NH_4ReO_4 have been studied using neutron powder diffraction (NPD) and Density Functional Theory (DFT), respectively. Despite the large incoherent background in the experimental NPD, associated with the presence of hydrogen, accurate and precise structural parameters were obtained. Comparison of the results of the NPD and DFT studies shows that the observed anomalous thermal contraction in NH_4ReO_4 is a consequence of thermally induced rotational

disorder of the NH_4 groups. Comparing the experimentally determined and optimized structures reveals deformation of the NH_4 tetrahedra that is responsible for the unusual tetragonal distortion of this material. The Raman Spectra of NH_4ReO_4 is presented and the modes are assigned based on the DFT calculations.

Introduction

Matching the thermal expansion of materials in modern devices can be critical to their overall performance and durability in applications such as aerospace technologies, optics, medical implants, fuel cells and electronics.[1-3] Understanding the mechanism and origin of thermal expansion is an essential step in designing matched materials. Materials with the tetragonal (space group $I4_1/a$) ABO_4 scheelite structure display strongly anisotropic thermal expansion and provide fertile ground to study thermal expansion.[4] The anisotropic thermal expansion in scheelite compounds was first described by Bayer almost 50 years ago, who noted that scheelites invariably display higher thermal expansion in the *c*-direction than in the *a*-direction.[5] This is believed to be a consequence of differences in the ordering of the two cations in the *a*- and *c*-directions which results in layered-type arrangement.[6] Two-dimensional layered oxides are well known to display much higher thermal expansion in the direction perpendicular to the layers.

The thermal expansion of NH_4ReO_4 is anomalous below room temperature, exhibiting large positive thermal expansion of the tetragonal *c*-axis but negative expansion of the *a*-axis resulting in near zero thermal expansion in the unit cell volume just below room temperature.[7, 8] Above room temperature, positive thermal expansion is observed for both the *a*- and *c*-axis. An early X-ray diffraction study by Kruger and Reynhardt revealed large rotational motion of the NH_4 group at room temperature that precluded location of the hydrogen atoms.[9] The hydrogen atoms were unambiguously located at low temperatures, 135 K. Swainson and Brown employed neutron diffraction methods in revisiting the problem and postulated that the behaviour is a consequence of temperature dependent orientational disorder of the ND_4 group.[10]

The motion of atoms in a crystal is of fundamental interest, and it is typically quantified by the atomic displacement parameters (ADPs) in crystallographic studies. Neutrons are scattered isotropically because of the short range, compared with the wavelength of the neutron, of the nuclear interaction between the neutron and the nucleus. This makes neutron

diffraction sensitive to small displacements of atoms from their equilibrium position, providing sensitivity to the ADPs. The isotropic description of the mean atomic displacements routinely used in analysis of powder X-ray diffraction data is only a very crude approximation of the motion. In favourable cases neutron diffraction allows the anisotropy of the displacements to be determined potentially providing insight into the thermal motion of the atoms and the translational and librational frequencies.

Because of the weak X-ray scattering power of hydrogen, neutron diffraction has the advantage over X-ray diffraction for elucidating structures incorporating light atoms such as hydrogen, in the presence of heavy atoms. Unfortunately, the incoherent scattering from hydrogen coupled with the relatively low fluxes available at neutron sources, has led to the general view that powder neutron diffraction is not suitable for hydrogen containing materials. The incoherent background can be avoided by deuteration, replacing ^{1}H isotope with deuterium ^{2}H, which has a much lower incoherent neutron scattering cross-section. Hydrogen and deuterium have different signs of their coherent neutron scattering lengths (-3.7406 fm and 6.671 fm, respectively), consequently incomplete deuteration can make the location of hydrogen more difficult by producing an effectively null, or near to null, scattering site. Consequently, the use of powder neutron diffraction methods to study the structure of hydrogen containing materials remains exceptional.

Studies over the past decade have demonstrated that the high incoherent background due to the presence of hydrogen, can be described by an angular dependent analytical function enabling separation of the coherent and incoherent contributions to the diffraction pattern. This is particularly the case when high resolution monochromatic data is obtained.[11, 12]

In the present paper we have used neutron powder diffraction to carry out a detailed study of the thermal expansion behaviour of NH_4ReO_4. These experimental studies have been supplemented with DFT calculations.

Experimental and Computational Details

The sample of NH_4ReO_4 (> 99%) was purchased from Aldrich and used as received. Neutron powder diffraction (NPD) measurements were performed on the high-resolution powder diffractometer Echidna at the Open Pool Australian Lightwater (OPAL) reactor, operated by the Australian Nuclear Science and Technology Organisation (ANSTO).[13] The sample was housed in a vanadium can placed within a cryostat. The data were collected over

the range 5° < 2θ < 162° with a step size of 0.05° at a wavelength of 1.6210 Å. Synchrotron X-ray powder diffraction data were collected over the angular range 5 < 2θ < 85°, using X-rays of wavelength 0.58921 Å, as determined by structural refinement of NIST SRM660b LaB_6 standard, on the powder diffractometer at beamline BL-10 of the Australian Synchrotron [14]. No impurities were detected in the S-XRD measurements.

Structure refinements, by the Rietveld method, were carried out using the GSAS program with the EXPGUI front-end.[15, 16] The peak profiles were modelled using a pseudo-Voigt function with GSAS function 4, and the background was estimated using a 15-term shifted Chebyshev function. The scale factor, detector zero-point, lattice parameters, atomic coordinates and atomic displacement parameters were refined together with the peak profile parameters.

Raman spectroscopy was undertaken using a Renishaw inVia Reflex Microscope under ambient conditions. A 622 nm laser was run at 1% intensity to measure $100 < \nu < 3200$ cm^{-1}, with three sets of 30 sec acquisitions to improve the signal-to-noise ratio. The spectral resolution was 0.3 cm^{-1}. The statistical occupation of thermal states was accounted for by scaling each intensity by the Bose-Einstein occupation factor.[17]

Calculations were performed with projector augmented wave (PAW) method using the Vienna *ab initio* simulation package (VASP), version 5.4.4.[18-20] The self-consistent ground state of the system was determined using the conjugate gradient technique to minimize the total energy of the system with respect to the plane-wave coefficients. The electronic wave functions were obtained by a density-mixing scheme and the structures were relaxed using the Broyden, Fletcher, Goldfarb, and Shannon method (BFGS).[21] The experimental crystal structure of NH_4ReO_4 was first relaxed to allow the ionic configurations, cell shape, and volume to change at ambient pressure. A plane-wave energy cut-off of 900 eV was used to ensure a high precision in the calculations. Brillouin zone sampling was performed using the Monkhost–Pack scheme[22] with a *k*-point grid of 4×4×2. The lattice constants and the atomic coordinates were optimized until the convergence of the force on each atom is less than 0.001 eV/Å. The exchange and correlation energies were taken as the generalized gradient approximation (GGA).[23] Different schemes of van der Walls (vdW) interaction were used to accurately capture the ground state volume and lattice constants with respect to the experimental values. The convergence criteria for the total energy and ionic loops were set to 10^{-8} eV and 10^{-5} eV Å, respectively. The valence electronic configurations for H, N, O, Re used in the calculations were $1s^1$, $2s^2\,2p^3$, $2s^2\,2p^6$ and $4f^{14}\,5d^5\,6s^2$, respectively.

Initially, lattice-dynamics calculations of the phonon modes for the tetragonal ($I4_1/a$) structure were performed at the zone center (Γ point) of the Brillouin zone (BZ) using VASP within the finite displacement method. The required force constants were computed within the Hellman-Feynman framework, on various atoms in different configurations of a supercell size of 3×3×1 with the optimized structure. The phonopy software (version 2.15.1) was used to estimate phonon frequencies in the entire Brillouin zone as a subsequent step to density functional calculations.[24]

Results and Discussion:

1. **Structure:**

The neutron powder diffraction (NPD) pattern of NH_4ReO_4 was well fitted to the tetragonal $I4_1/a$ scheelite model described previously [8, 10] and examples of the fitted profiles are given in Figure 1. This figure highlights the large angular dependent background due to the incoherent scattering associated with the use of a hydrogenated sample. The flat difference profiles demonstrate that the shifted Chebyshev function successfully modelled the background. The refined cell parameters (a = 5.88235(11) Å, c = 12.96132(29) Å) for the data measured at room temperature, listed in Table 1, are in reasonably good agreement with our previous synchrotron X-ray diffraction study.[8] The structure was refined using origin choice 2 of space group $I4_1/a$ in which the Re cations are at the 4*a* special position (0 1/4 1/8), the nitrogen atom of the ammonium ion is located at the 4*b* special position (0 1/4 5/8) and the oxygen and hydrogen atoms are at 16*f* (*x, y, z*) general positions. Eight ReO_4 oxygens surround the NH_4 ions in the NH_4ReO_4 structure, four of which are axial and four of which are equatorial to the ammonium ions. Despite the large background, the esds for the refined positional parameters of both the oxygen and hydrogen atoms were unexceptional, see Table S1. The inclusion of anisotropic atomic displacement parameters for the oxygen and hydrogen atoms resulted in a noticeable improvement in the fit, χ^2 decreased from 2.64 to 1.61 for the profile measured at room temperature. The relative intensity of the higher angle reflections increases noticeably upon cooling from room temperature (RT) to 3 K as a consequence of decreased displacements, see Figures 1 and S1. As evident from Tables S1 and S2 this is predominantly due to a dramatic decrease in the ADPs of the hydrogen atom.

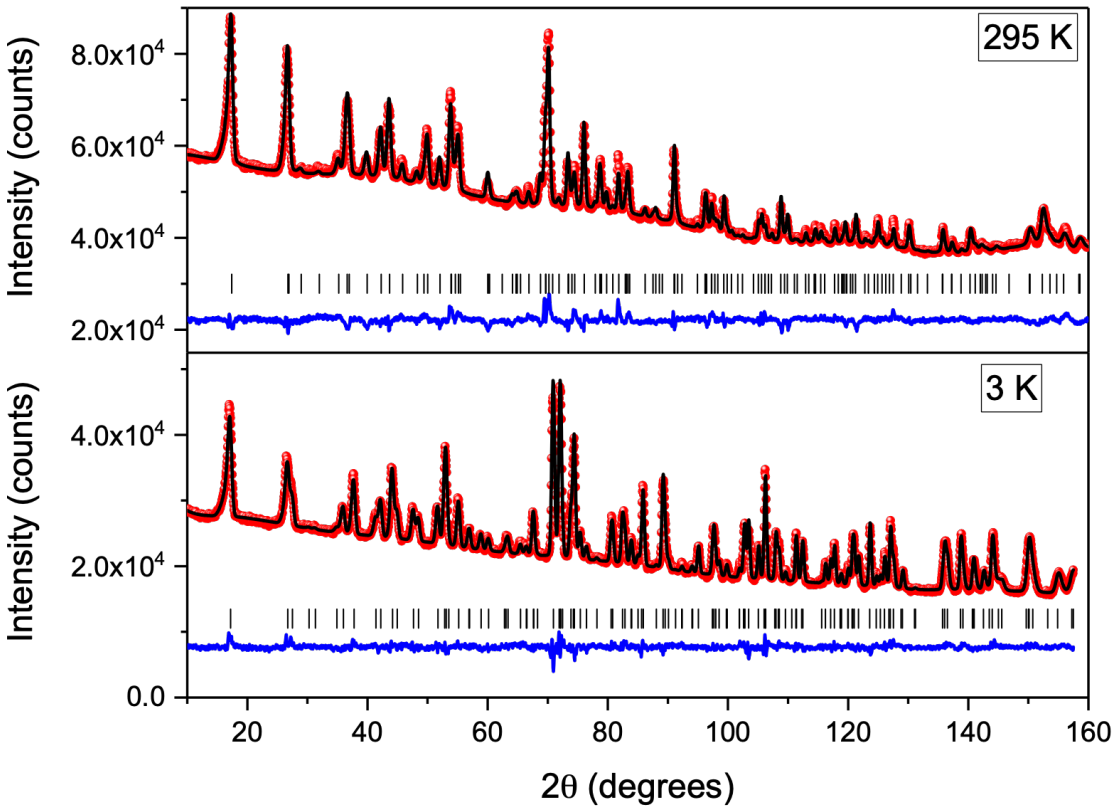

Figure 1. Representative Rietveld profiles for neutron powder diffraction data from NH_4ReO_4 measured at 295 and 3 K. The red symbols are the measured profiles, and the solid black line is the calculated profile. The lower continuous blue line is the difference profile, and the tick marks show the positions of the space group allowed Bragg reflections. The patterns were collected with $\lambda = 1.6210$ Å. The high angular dependent background arises from the presence hydrogen in the samples.

The refined structures at 3 and 295 K are compared in Figure 2. The most dramatic difference is the large increase in the magnitude of the APDs of the hydrogen atoms, which occurs between 150 and 200 K, Table S2. This apparently corresponds to the broad maximum in the molar heat capacity reported by Weir and Staveley.[25] This figure illustrates that large displacement of the hydrogen atoms is taking place in the *ab*-plane with the displacement toward the nitrogen atom being significantly less than perpendicular to the N-H bond. This sort of behaviour is not uncommon for molecular framework materials, since the lowest energy vibrational modes usually involve transverse displacements.[26]

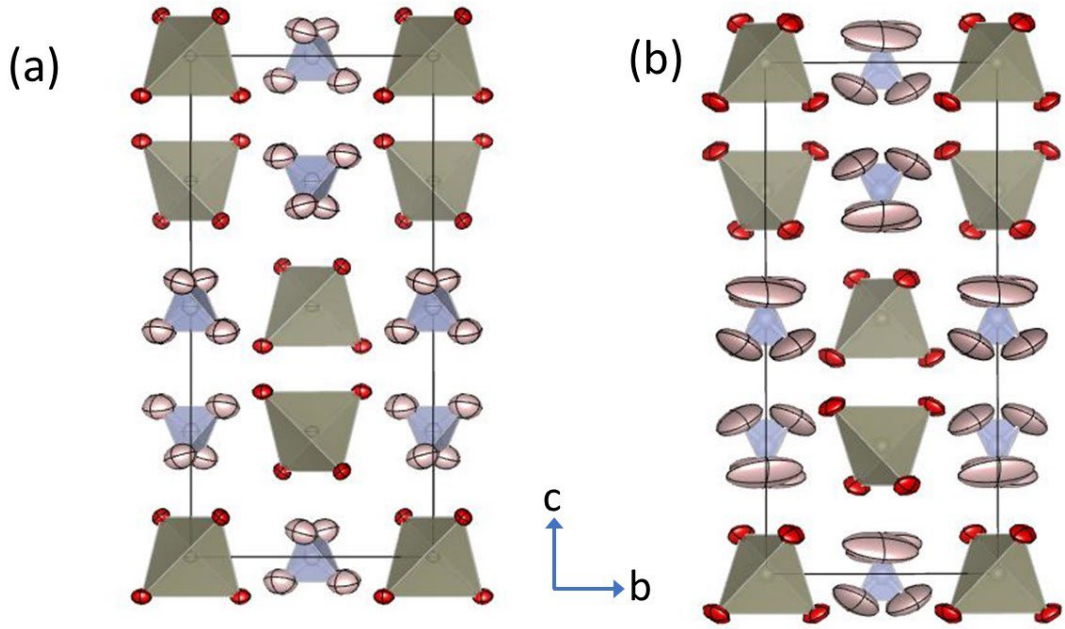

Figure 2. Comparison of the structure of $(NH_4)ReO_4$ at (a) 3 K and (b) 295 K. The figure highlights the large anisotropic displacement parameters of the hydrogen atoms.

The temperature dependence of the lattice parameters is illustrated in Figure 3 and shows excellent agreement between the current work and the earlier S-XRD study. Notably, this figure illustrates the positive thermal expansion of the tetragonal *c*-axis but negative expansion of the *a*-axis resulting in near-zero thermal expansion in the unit cell volume. The linear Thermal Expansion Coefficients (TEC) between 150 and 250, estimated as $\alpha_i = \frac{1}{i_{150}}\left(\frac{\Delta i}{\Delta T}\right)$ where i is the parameter of interest and T the temperature, were α_a = -147.5 x 10^{-6} $ÅK^{-1}$, α_c = 299.2 x 10^{-6} $ÅK^{-1}$ and α_{Vol} = 3.7402 x 10^{-6} $Å^3K^{-1}$. The Re-O bond distances (1.730(2) Å at 295 K) and O-Re-O angles 108.77(8) and 110.88(17) º are essentially independent of temperature and demonstrating the rigid nature of the ReO_4 tetrahedra. Conversely, there appears to be a dramatic shortening of the N-H bond from 1.032(3) to 0.882(5) Å upon heating from 3 to 295 K, with a concurrent apparent increase in the distortion of the NH_4 tetrahedra, see Table 2. It is believed that this is a consequence of a dramatic increase in the libration of the hydrogen atoms. Essentially the hydrogen atoms show approximately circular rotation. This motion is fitted as an ellipsoid when anisotropic displacement parameters are used and the atom appears to lie at the centre of the circle of motion, rather than on its periphery. This effect makes the bond distance appear shorter than they actually are. This effect is analogous to the transverse motion in rigid unit modes associated with Negative Thermal Expansion

(NTE).[27, 28] Swainson and Brown employed rigid body constraints in their earlier study of $(ND_4)ReO_4$ to prevent this anomalous shortening of the N-D bonds, constraining the N-D distance to be 1.025 Å. They modelled the large libration of the D(H) atoms using a split site model.[10]

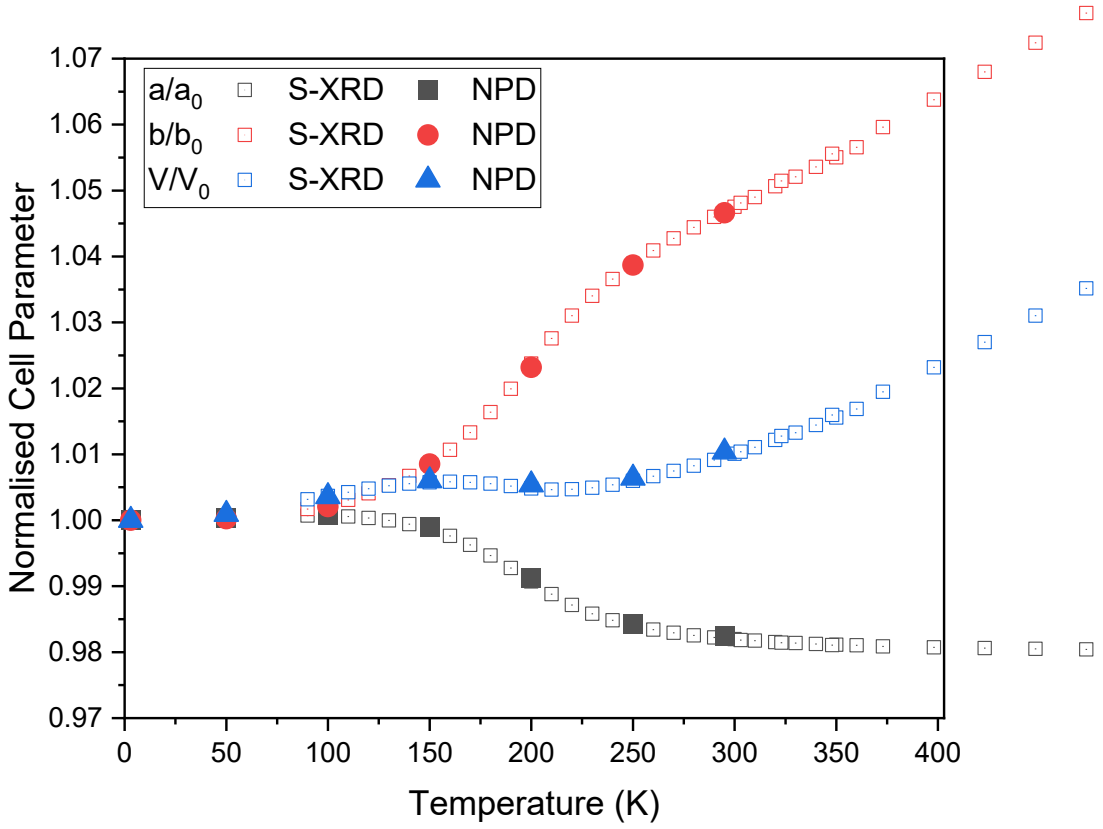

Figure 3. Temperature dependence of the normalised unit cell parameter and volume obtained by Rietveld refinement against neutron (red squares) and Synchrotron X-ray (back circles) data for NH_4ReO_4.[8] The cell parameters were normalised to the corresponding value obtained from the NPD at 3K.

To further probe the rigid nature of the NH_4 and ReO_4 tetrahedra, separate translation-libration-screw (TLS) [29, 30] refinements and maximum entropy method (MEM) analysis was undertaken. These methods are seen as complementary, as TLS described the translation, libration and screw-rotation displacement of a pseudo-rigid body and MEM constructs an electron/nuclear density map on a three-dimensional grid instead of using atomic positions.

Figure 4 details the similarity between the TLS and MEM models of NH_4ReO_4 based on the room temperature NPD data. Of interest is the density shape around the O and H atoms, displaying a distribution that is reasonably close to an ellipsoid. This suggests that Rietveld refinements with anisotropic ADPs are a reasonably accurate approximation.

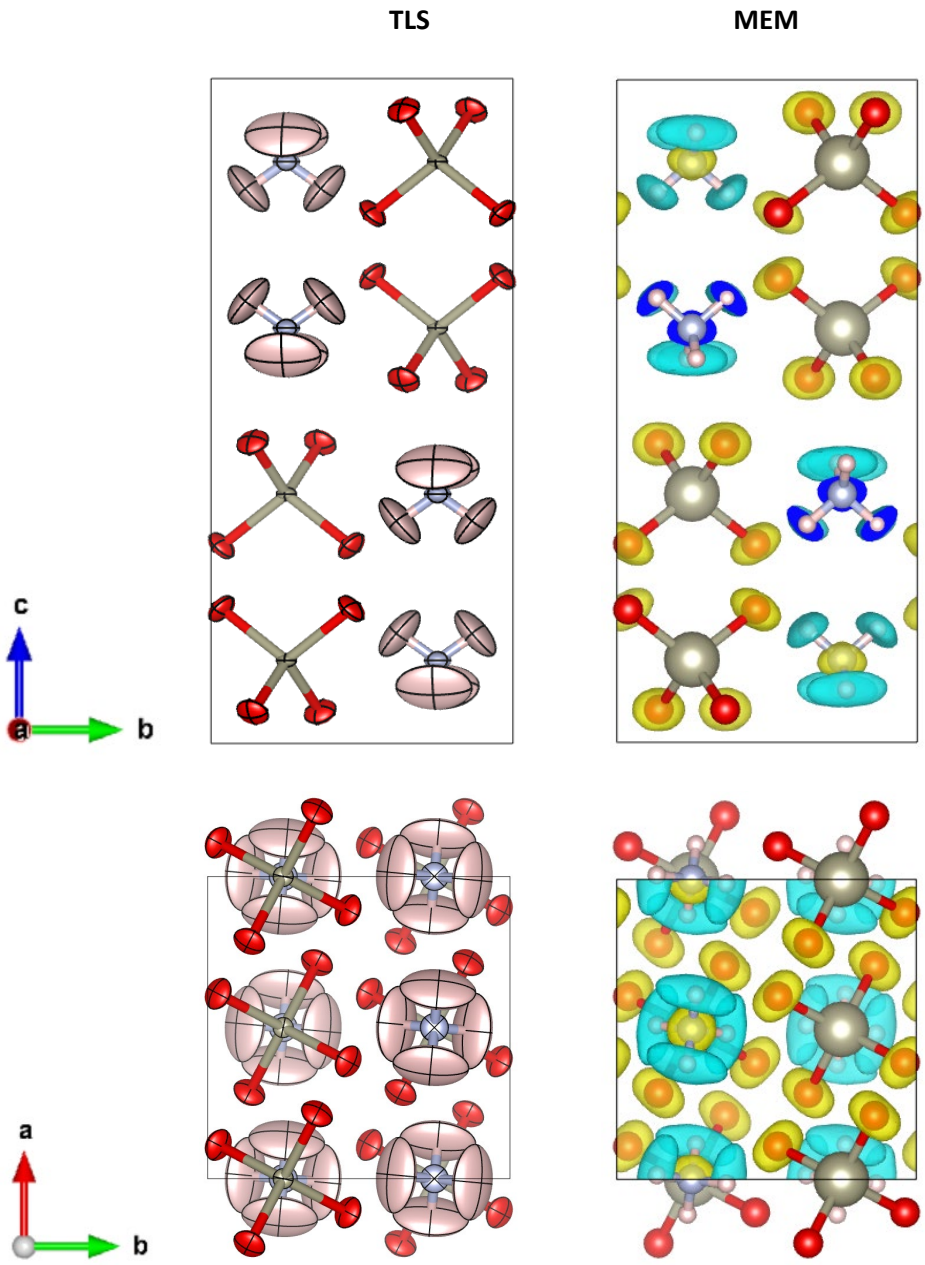

Figure 4: (Left) The translation-libration-screw (TLS) and (Right) maximum entropy method (MEM) plots, based on the room temperature NPD data of NH_4ReO_4.

Recently, Brutchey and co-workers described an analogous shortening of the Mo-O bonds in the AMoO4 scheelites.[31] Using total scattering methods and pair distribution function analysis they showed that this was a consequence of static orientational disorder of the MoO_4 tetrahedra. Orientational disorder in scheelites is not unexpected since these have an open framework structure that affords a large amount of structural flexibility. In the molybdates described by Brutchey the orientational disorder is predominantly static and the MoO_4

tetrahedra appear to be randomly rotated throughout the lattice.[32] Lack of correlation between the tetrahedra leads to conventional thermal expansion behaviour.[33] Conversely concerted rotation of tetrahedra coupled with large transverse displacements as observed in the $A_2(MoO_4)_3$ system leads to negative thermal expansion.[34] The observation of anomalous thermal expansion behaviour in NH_4ReO_4 demonstrates the correlation between the rotational disorder of the ammonia groups as evidenced from the large atomic displacement parameters observed in the present work.

2. Ground state structural properties:

The lattice constants and atomic positions for NH_4ReO_4 were optimized as a function of normal stress by minimizing the total energy. The calculated values of the lattice parameters of NH_4ReO_4 are presented in Table 3 and these should be compared to the experimental values obtained for the refinement using data measured at 3 K given in Table 1. The structure at 3 K represents the most appropriate benchmark for the calculations, since at this temperature disorder of the NH_4^+ groups is minimal, further the DFT calculations ignore thermal effects, *i.e.,* they are most appropriate to the low temperature structure. The calculated lattice constants, a = 5.77 Å and c = 13.21 Å with the optB88-vdW functional show 1.87% and 1.67% deviation respectively from the experimental value for the 3 K structural refinement. The other van der Walls (vdW) schemes show slightly larger deviations either in the a or c lattice parameters due to the different calculation methods. The agreement between the calculated and observed (3 K) cell volume is 0.83%. This shows the reliability of our present DFT based first – principles calculations.

The thermal expansion of NH_4ReO_4 obtained from the DFT calculations within the harmonic approximation is illustrated in Figure 5. Comparing the linear TEC between 150 and 250 K (where the greatest change is evident in the experimental observation) we obtain α_a = 24.92 x 10^{-6} vs -147.5 x 10^{-6} ÅK^{-1} and α_c = 56.77 x 10^{-6} vs 299.2 x 10^{-6} ÅK^{-1}. As generalised by Bayer for the scheelites the calculations show larger TEC in the c-direction than in the a-direction.[5] This figure illustrates a number of important features. Firstly, both the unit cell parameters and the cell volume plateau at low temperatures due to thermal depopulation of the excited states. This low temperature plateau in the cell parameters extends to about 50 K, whereas in the experimental study the plateau extends to around 120 K as shown in Figure 3. The calculated behaviour in terms of both the appearance of the low temperature plateau and the relative expansion of the a- and c-axis is, however, very similar to the thermal expansion behaviour of the isostructural oxides $PbMoO_4$ [35] and $CaWO_4$ [4]. As experimentally observed

for these two oxides, the calculated temperature dependence of the *c*-axis is greater than that of the *a*-axis reflecting the layered structural arrangement. Secondly, the calculated unit cell values are typically in good agreement with those observed at 3 K. A more subtle effect is in the difference in the absolute values. Irrespective of the functional used the calculations fail to reproduce the observed *c*/*a* ratio. Invariably the calculated *c*/*a* ratio was larger than the observed value of 2.068, noting that the calculated *c*/*a* values fall over a relatively narrow range 2.280 – 2.390. In other $A$$ReO_4$ (A = Ag, Na, K, Rb) scheelites the observed *c*/*a* value is ~ 2.2-2.3.[36] In brief the DFT calculations in the harmonic approximation neither predict the anomalies in the thermal behaviour nor the unusual reduction in the *c*/*a* value. The former arises since DFT does not consider the anharmonicity and effect of rotational disorder of the NH_4 and/or ReO_4 groups. The latter is more interesting and implies an unusual contraction in the *c*-parameter.

Further evidence of the impact of the rotational disorder of the NH_4 and/or ReO_4 groups is seen by comparison of the calculated heat capacity, that in contrast to the earlier experimental report by Weir and Stavely, does not provide any evidence for any anomalous behaviour. This suggests that the experimentally observed behaviour is associated with disorder that is not modelled by the DFT lattice-dynamics calculations.

The DFT-optimized atomic coordinates for the H and O atoms are compared with the 3 K experimental values in Table 4. Although the agreement appears to be only fair, especially for the hydrogen atom, the calculated bond distances for Re-O 1.759 versus 1.7346 (14) Å (1.4%) and N-H 1.037 versus 1.032 (3) Å (- 0.5%) are in good agreement. The bond angles in the ReO_4 tetrahedra are unexceptional the observed values being 108.8(1) and 110.8(1)º compared with the calculated values of 110.0 and 109.2 º reflecting the rigid nature of the ReO_4 groups. The calculated bond angles for the NH^+ groups suggest a regular tetrahedra, 110.9 and 108.8 º whereas the observed angles 106.4(3) and 111.0(2)º point to a more distorted environment. Evidently the NH_4^+ group is softer and more easily deformed than the ReO_4 groups and it is postulated that this deformation contributes to the contraction in the *c*-axis and the observed reduction in the *c*/*a* ratio.

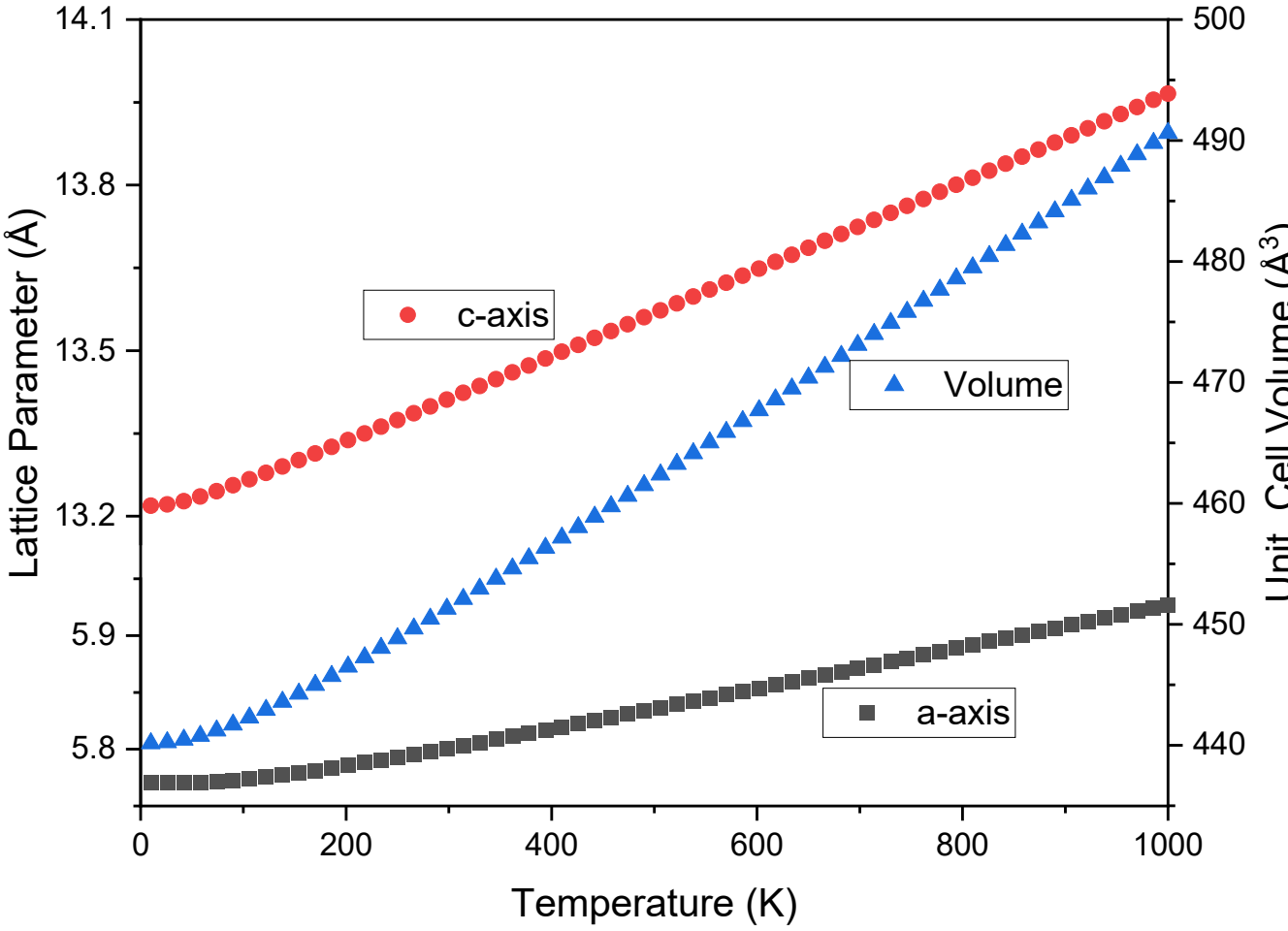

Figure 5. Calculated thermal expansion of the lattice parameters and unit cell volume for NH_4ReO_4

Table 1. Refined lattice parameters and associated measures of fit for NH_4ReO_4 obtained by Rietveld refinements against power neutron diffraction data.

Temp	*a* (Å)	*c* (Å)	Vol (Å^3)	χ^2	R_{wp}	R(F^2)
3	5.98696 (6)	12.38398(17)	443.887(9)	2.10	0.015	0.065
50	5.98898 (7)	12.38698(17)	444.295(9)	1.94	0.014	0.045
100	5.99152 (7)	12.40948(19)	445.480(10)	1.73	0.013	0.041
150	5.98135 (8)	12.48939(21)	446.555(12)	1.57	0.013	0.050

200	5.93468 (9)	12.67100(24)	446.278(13)	1.51	0.012	0.057
250	5.89314(10)	12.86305(27)	446.722(14)	1.47	0.012	0.066
295	5.88235(11)	12.96132(29)	448.488(15)	1.59	0.011	0.083

Table 2. Selected interatomic distances and angles for NH_4ReO_4 estimated by Rietveld refinements against power neutron diffraction data.

Temp (K)	Re-O (Å)	N-H (Å)	O-H (Å)	O-H (Å)	O-Re-O (º)	O-Re-O (º)	H-N-H (º)	N-N-H (º)
3K	1.7346(14)	1.032(3)	1.856(3)	2.652(4)	108.8(1)	110.8(1)	106.4(3)	111.0(2)
50K	1.7326(14)	1.031(3)	1.862(3)	2.654(4)	108.81(5)	111.0(1)	106.0(3)	111.2(2)
100	1.7284(15)	1.015(3)	1.889(3)	2.657(4)	108.46(6)	111.5(1)	106.0(4)	111.3(2)
150	1.7309(17)	1.013(3)	1.890(3)	2.677(4)	108.62(6)	111.19(12)	104.3(4)	112.1(2)
200	1.735(2)	0.983(4)	1.920(5)	2.640(8)	109.47(8)	109.14(15)	103.2(5)	112.7(3)
250	1.719(2)	0.945(6)	2.060(9)	2.412(11)	108.84(9)	110.74(17)	98.4(8)	115.3(4)
295	1.730(2)	0.882(5)	2.123(10)	2.413(12)	108.77(8)	110.88(17)	94.8(8)	117.3(5)

Table 3. Comparison of the lattice constants (*a*, *c* in Å) and Volume (V in $Å^3$), of NH_4ReO_4 calculated with different vdW-DF functionals. The percentage error from the experimental value observed at 3K is given.

Functional	*a*(Å)	*c*(Å)	Volume($Å^3$)	c/a
DFT-D2	5.682	12.954	418.35(-5.75%)	2.280
DFT-TS	5.736	13.679	450.20(1.42%)	2.385

optPBE	5.807	13.562	457.426(3.05%)	2.335
optB88-vdW	5.7716	13.213	440.164(-0.83%)	2.289
optB86-vdW	5.754	13.265	439.254(-1.04%)	2.305
rev-vdW-DF2	5.885	13.941	482.864(8.78%)	2.369
D3(IVDW=11)	5.707	13.640	444.327(-0.10%)	2.390
D3-BJ(IVDW=12)	5.726	13.505	442.971(-0.21%)	2.359
Experiment	5.98695(6)	12.3840(2)	443.885(12)	2.068

Table 4. Comparison of the calculated (with the optB8-vdW correction) and observed atomic coordinates for NH_4ReO_4. The observed values correspond to refinements of NPD data measured at 3 K.

Atoms	Expt./Theo.	*x*	*y*	*z*
H	Expt.	0.1312(5)	0.2072(7)	0.5751(2)
	Theory.	0.0940	0.1357	0.5805
O	Expt.	0.1236(2)	0.0462(2)	0.2045(1)
	Theory.	0.1222	0.0323	0.2013
N	Expt.	0.00	0.25	0.625
	Theory.	0.00	0.25	0.625
Re	Expt.	0.00	0.25	0.125
	Theory.	0.00	0.25	0.125

3. Phonon Dispersion:

Table 3 illustrates the importance of the vdW functionals to accurately reproduce the experimental lattice parameters, where the OptB88-vdW functional performs best.

Consequently, this was used to compute the full phonon dispersion of NH_4ReO_4 along the high symmetry points of the Brillouin zone (Γ-M-X-P-N-Γ) as illustrated by Figure 6. Since there are 40 atoms per unit cell, the phonon spectra have a total of 120 branches (including three acoustic) associated with three degrees of freedom. All phonon modes exhibit real frequencies in the Brillouin zone path, suggesting dynamical stability of the optimized NH_4ReO_4 structure. To further understand atomic-specific contributions to phonon modes, we calculated the total and partial phonon density of states for NH_4ReO_4 (Figure 6). The mass difference between the H, N, O, and Re atoms results in the three optical gaps seen in Figure 6. The Re atom dynamics are the major contributor to the acoustic region (0 to 10 meV), whereas the lighter H atoms contribute to the entire spectral regime. Although the atomic masses of oxygen and nitrogen are similar the optical modes of these are distinct, with the optical modes for nitrogen detected around 160 and 180 meV and those for oxygen around 110 to 125 meV. This clearly indicates that as the atomic mass decreases, the vibrational modes increase in energy.

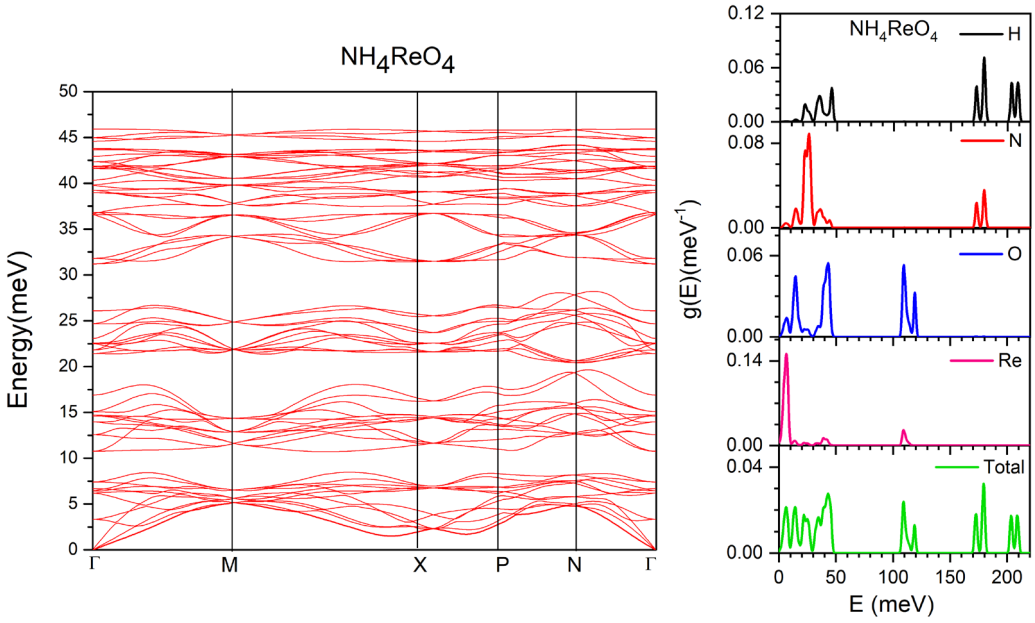

Figure 6. Phonon Dispersion along high symmetry points of the Brillouin zone *(Γ-M-X-P-N-Γ)* and total and partial phonon density of states of NH_4ReO_4. These were calculated using the optB88-vdW functional.

4. Raman Spectra:

The Raman spectra of NH_4ReO_4, shown in Figure 7, contains two sets of relative intense peaks, near 900 cm^{-1} associated with stretching modes of the ReO_4 moiety and near

350 cm^{-1} due to bending modes of the ReO_4.[37, 38] There are weaker peaks near, 1418, 1666 and 3151 cm^{-1}, arise from either stretching or bending modes of the NH_4 groups.[39] The DFT calculations facilitate assignment of the individual modes. The peak at 965 cm^{-1} is due to the symmetric υ_1 stretching mode and that at 891 cm^{-1} is from the antisymmetric υ_1 stretching mode. These are described by the irreducible representations (*irreps*) A_g and E_g respectively. There is a second antisymmetric (υ_3 – B_g) stretching mode at 913 cm^{-1}. The feature near 350 cm^{-1} contains contributions from four different modes (1 x A_g 1 x E_g and 2 x B_g). The calculations show that three of these are, within the resolution of the measurements, degenerate leading to the appearance of a single peak with a shoulder. The observed frequencies are very similar to the values reported for $NaReO_4$ and $KReO_4$ reflecting the rigid nature of the ReO_4 groups. Gassman *et al.*[37] postulated that small shifts in the mode frequencies are a result of changes in the covalency experienced by the ReO_4 groups as the nature of the nearest neighbours changes.

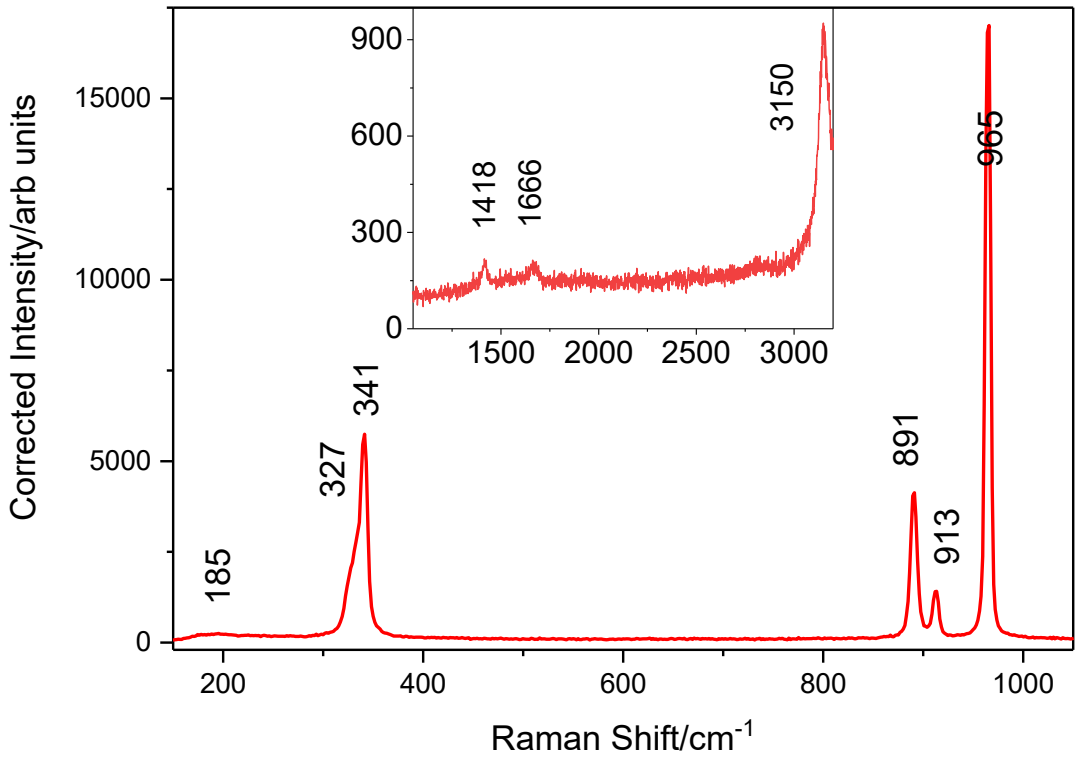

Figure 7. Raman Spectra of crystalline NH_4ReO_4 measured using 622 nm Laser. The inset illustrates the weaker high frequency modes associated with the stretching or bending modes of the NH_4 groups.

Table5. The Calculated vibrational modes and observed Raman modes of NH_4ReO_4. The Raman spectra were measured between 150 and 3200 cm^{-1}

Irreps	Calculated (cm^{-1})	Observed (cm^{-1})
Au	0	
Eu	0	
Bg	53.8	Not Measured
Eg	59.8	
Eu	86.8	
Ag	117.7	Not Observed
Eg	118.6	Not Observed
Bu	136.3	
Eu	175.9	
Eg	181.5	185
Au	186.0	
Bg	210.5	Not Observed
Eu	256.4	
Eg	295.1	Not Observed
Au	295.6	
Eu	316.4	
Bg	325.3	327
Bg	335.7	341
Ag	337.2	341
Eg	337.8	341

Bu	346.3	
Au	352.0	
Bu	359.6	
Ag	370.4	Not Observed
Au	867.0	
Eg	876.0	891
Eu	883.3	
Bg	896.6	913
Ag	956.0	965
Bu	957.7	
Bg	1384.9	Not observed
Au	1388.1	
Eu	1436.7	
Eg	1447.7	1418
Ag	1639.2	1666
Bu	1659.5	
Au	1680.3	
Bg	1692.4	1666
Ag	3204.3	3151?
Bu	3214.9	
Au	3247.9	
Bg	3251.4	3151?
Eu	3256.8	
Eg	3257.6	3151?

Conclusions

Using variable temperature high resolution neutron powder diffraction (PND) methods, we have demonstrated that the anomalous thermal expansion in NH_4ReO_4 is a consequence of thermally induced rotational disorder of the NH_4 groups. This was modelled using anisotropic displacement parameters. Maximum Entropy Method analysis of the PND profile measured at room remperature confirmed the absence of local maxima in the nuclear density, showing the split atom model previously proposed by Swanson and Brown[10] was unnecessary. Density Functional Theory was used to study the ground state of NH_4ReO_4. We found the optB88-vdW functional calculated for the Generalised Gradient Approximation captured the low temperature (3 K) volume but failed to reproduce the experimentally observed tetragonal *c*/*a* ratio. This reflects deformation of the NH_4 tetrahedra. The DFT calculations facilitated assignment of the experimentally observed Raman modes.

Acknowledgements

Funding is gratefully acknowledged from the Australian Research Council. We thank ANSTO's Australian Centre for Neutron Scattering for instrument time. This research was facilitated by access to Sydney Analytical, a core research facility at the University of Sydney. MSM gratefully acknowledges the financial support from the Comunidad de Madrid, Spain, through an "Atracción de Talento Investigador" fellowship (2020-T2/IND-20581). BM thanks the Australian Institute of Nuclear Science and Engineering for a scholarship. JPK would like to thank Defense Research and Development Organization (DRDO), Ministry of Defense, Govt. of India for the financial support under grant No.DRDO/18/1801/2016/01038:ACREHM-PHASEIII. G.V acknowledges acknowledges the Institute of Eminence, University of Hyderabad UoH-IoE-RC3-21-046 for funding and the CMSD, University of Hyderabad, for providing the computational facilities.

References

1. Chen, J.; Hu, L.; Deng, J. X.; Xing, X. R., Negative thermal expansion in functional materials: controllable thermal expansion by chemical modifications. *Chemical Society Reviews* **2015,** *44* (11), 3522-3567.
2. Mahato, N.; Banerjee, A.; Gupta, A.; Omar, S.; Balani, K., Progress in material selection for solid oxide fuel cell technology: A review. *Progress in Materials Science* **2015,** *72*, 141-337.
3. Takenaka, K., Negative thermal expansion materials: technological key for control of thermal expansion. *Science and Technology of Advanced Materials* **2012,** *13* (1), 013001.
4. Senyshyn, A.; Hoelzel, M.; Hansen, T.; Vasylechko, L.; Mikhailik, V.; Kraus, H.; Ehrenberg, H., Thermal structural properties of calcium tungstate. *Journal of Applied Crystallography* **2011,** *44*, 319-326.
5. Bayer, G., Thermal-expansion of ABO_4-compounds with zircon and scheelite structures. *Journal of the Less-Common Metals* **1972,** *26* (2), 255-&.
6. Kennedy, B. J.; Injac, S.; Thorogood, G. J.; Brand, H. E. A.; Poineau, F., Structures and Phase Transitions in Pertechnetates. *Inorganic Chemistry* **2019,** *58* (15), 10119-10128.
7. Powell, B. M.; Brown, R. J. C.; Harnden, A. M. C.; Reid, J. K., Thermal effects in the structure of ammonium perrhenate. *Acta Crystallographica Section B-Structural Science* **1993,** *49*, 463-468.
8. Reynolds, E. M.; Yu, M.; Thorogood, G. J.; Brand, H. E. A.; Poineau, F.; Kennedy, B. J., Thermal expansion of ammonium pertechnetate and ammonium perrhenate. *Journal of Solid State Chemistry* **2019,** *274*, 64-68.
9. Kruger, G. J.; Reynhardt, E. C., Ammonium perrhenate at 295-K and 135-K. *Acta Crystallographica Section B-Structural Science* **1978,** *34* (JAN), 259-261.
10. Swainson, I. P.; Brown, R. J. C., Refinement of ammonium perrhenate structure using a pseudo-spin model for the ammonium ion orientation. *Acta Crystallographica Section B-Structural Science* **1997,** *53*, 76-81.
11. Weller, M. T.; Henry, P. F.; Ting, V. P.; Wilson, C. C., Crystallography of hydrogen-containing compounds: realizing the potential of neutron powder diffraction. *Chemical Communications* **2009,** (21), 2973-2989.
12. Xue, Z. L.; Ramirez-Cuesta, A. J.; Brown, C. M.; Calder, S.; Cao, H. B.; Chakoumakos, B. C.; Daemen, L. L.; Huq, A.; Kolesnikov, A. I.; Mamontov, E.; Podlesnyak, A. A.; Wang, X. P., Neutron Instruments for Research in Coordination Chemistry. *Eur. J. Inorg. Chem.* **2019,** (8), 1065-1089.
13. Avdeev, M.; Hester, J. R., ECHIDNA: a decade of high-resolution neutron powder diffraction at OPAL. *Journal of Applied Crystallography* **2018,** *51* (6), 1597-1604.
14. Wallwork, K. S.; Kennedy, B. J.; Wang, D., Australian Synchrotron Powder Diffractometer. *AIP Conference Proceedings* **2007,** *879*, 879.
15. Larson, A. C.; Von Dreele, R. B., GSAS. *General Structure Analysis System. LANSCE, MS-H805, Los Alamos, New Mexico* **1994**.
16. Toby, B. H., EXPGUI, a graphical user interface for GSAS. *J. Appl. Cryst.* **2001,** *34*, 210-213.
17. Mullens, B. G.; Avdeev, M.; Brand, H. E. A.; Mondal, S.; Vaitheeswaran, G.; Kennedy, B. J., Insights into the structural variations in $SmNb_{1-x}Ta_xO_4$ and $HoNb_{1-x}Ta_xO_4$ combined experimental and computational studies. *Dalton Transactions* **2021,** *50* (26), 9103-9117.
18. Kresse, G.; Furthmuller, J., Efficient iterative schemes for ab initio total-energy calculations using a plane-wave basis set. *Physical Review B* **1996,** *54* (16), 11169-11186.
19. Kresse, G.; Furthmuller, J., Efficiency of ab-initio total energy calculations for metals and semiconductors using a plane-wave basis set. *Computational Materials Science* **1996,** *6* (1), 15-50.
20. Kresse, G.; Joubert, D., From ultrasoft pseudopotentials to the projector augmented-wave method. *Physical Review B* **1999,** *59* (3), 1758-1775.
21. Fischer, T. H.; Almlof, J., General-methods for geometry and wave-function optimization. *Journal of Physical Chemistry* **1992,** *96* (24), 9768-9774.
22. Monkhorst, H. J.; Pack, J. D., Special points for brillouin-zone integrations. *Physical Review B* **1976,** *13* (12), 5188-5192.

23. Grimme, S., Semiempirical GGA-type density functional constructed with a long-range dispersion correction. *Journal of Computational Chemistry* **2006,** *27* (15), 1787-1799.
24. Togo, A.; Tanaka, I., First principles phonon calculations in materials science. *Scripta Materialia* **2015,** *108*, 1-5.
25. Weir, R. D.; Staveley, L. A. K., The heat-capacity and thermodynamic properties of potassium perrhenate and ammonium perrhenate from 8 K to 304 K. *Journal of Chemical Physics* **1980,** *73* (3), 1386-1392.
26. Chapman, K. W.; Chupas, P. J.; Kepert, C. J., Direct Observation of a Transverse Vibrational Mechanism for Negative Thermal Expansion in $Zn(CN)_{-2}$: An Atomic Pair Distribution Function Analysis. *Journal of the American Chemical Society* **2005,** *127* (44), 15630-15636.
27. Tallentire, S. E.; Child, F.; Fall, I.; Vella-Zarb, L.; Evans, I. R.; Tucker, M. G.; Keen, D. A.; Wilson, C.; Evans, J. S. O., Systematic and Controllable Negative, Zero, and Positive Thermal Expansion in Cubic $Zr_{1-}xSn_xMo_2O_8$. *Journal of the American Chemical Society* **2013,** *135* (34), 12849-12856.
28. Welche, P. R. L.; Heine, V.; Dove, M. T., Negative thermal expansion in beta-quartz. *Physics and Chemistry of Minerals* **1998,** *26* (1), 63-77.
29. Schomaker, V.; Trueblood, K. N., On the rigid-body motion of molecules in crystals. *Acta Crystallographica Section B* **1968,** *24* (1), 63-76.
30. Urzhumtsev, A.; Afonine, P. V.; Adams, P. D., TLS from fundamentals to practice. *Crystallography Reviews* **2013,** *19* (4), 230-270.
31. Rabuffetti, F. A.; Culver, S. P.; Suescun, L.; Brutchey, R. L., Structural Disorder in $A$$MoO_4$ (A = Ca, Sr, Ba) Scheelite Nanocrystals. *Inorganic Chemistry* **2014,** *53* (2), 1056-1061.
32. Culver, S. P.; Brutchey, R. L., Thermally activated rotational disorder in $CaMoO_4$ nanocrystals. *Crystengcomm* **2016,** *18* (24), 4485-4488.
33. Maji, B. K.; Jena, H.; Asuvathraman, R.; Kutty, K. V. G., Electrical conductivity and thermal expansion behavior of $M$$MoO_4$ (M = Ca, Sr and Ba). *Journal of Alloys and Compounds* **2015,** *640*, 475-479.
34. Tyagi, A. K.; Achary, S. N.; Mathews, M. D., Phase transition and negative thermal expansion in $A_2(MoO_4)_3$ system (A=Fe^{3+}, Cr^{3+} and Al^{3+}). *Journal of Alloys and Compounds* **2002,** *339* (1), 207-210.
35. Achary, S. N.; Patwe, S. J.; Vishwanath, A.; Wajhal, S.; Krishna, P. S. R.; Tyagi, A. K., Evolution of crystal structure of $PbMoO_4$ between 5 and 300 K: A low temperature powder neutron diffraction study. *Materials Chemistry and Physics* **2021,** *260*.
36. Chay, C.; Avdeev, M.; Brand, H. E. A.; Injac, S.; Whittle, T. A.; Kennedy, B. J., Crystal structures and phase transition behaviour in the 5d transition metal oxides $AReO_4$ (A = Ag, Na, K, Rb, Cs and Tl). *Dalton Transactions* **2019,** *48* (47), 17524-17532.
37. Gassman, P. L.; McCloy, J. S.; Soderquist, C. Z.; Schweiger, M. J., Raman analysis of perrhenate and pertechnetate in alkali salts and borosilicate glasses. *Journal of Raman Spectroscopy* **2014,** *45* (1), 139-147.
38. Mondal, S.; Vaitheeswaran, G.; Kennedy, B. J.; Chay, C.; Injac, S.; Errandonea, D., Crystal structure and phase transition of $TlReO_4$: a combined experimental and theoretical study. *Journal of Physics: Condensed Matter* **2020,** *33* (6), 065403.
39. Ohe, W. v. d., Raman spectrum of $(NH_4)_2TiF_6$ and trigonal Cs_2TiF_6 *The Journal of Chemical Physics* **1976,** *65* (9), 3575-3585.